Supporting Information

Foster et al. 10.1073/pnas.1206580109

SI Results

Task behavioral data are as follows: For the self-episodic condition, subjects on average responded false to the majority (73%) of trials (m "true" response trials = 13; m "false" response trials = 35). Mean reaction times (RTs) between true (m = 2.55 s) and false (m = 2.32 s) responses were not significantly different for the self-episodic condition [$t(14) = 0.57$, $P = 0.58$]. For the self-semantic condition, on average subjects responded equally true (m trials = 24) and false (m trials = 24) across trials, with no significant difference in mean RT [m RT true = 2.45 s; m RT false = 2.28 s; $t(12) = 0.47$, $P = 0.65$]. Conversely, subjects responded true more often (73%) than false in the self-judgment condition (true m trials = 35; false m trials = 12). Mean RT for this condition was not significantly different between true or false response trials [m RT true = 2.3 s; m RT false = 3.15 s; $t(12) = -0.91$, $P = 0.38$]. Finally, for the control math condition, there was a similar profile of behavior whereby subjects on average responded true more often (77%) than false to equations. Mean RT was greater for math trials judged to be false, but not significantly different from true trials [m RT true = 3.1 s; m RT false = 4.29 s; $t(14) = -1.46$, $P = 0.17$]. As described below, electrophysiological data were correlated with RT, but did not show any significant difference between true or false responses.

SI Materials and Methods

Anatomical Localization of Electrodes. As part of their clinical monitoring, subjects were implanted with differing montages of flexible strip and grid subdural platinum electrodes (AdTech Medical Instruments). Electrodes were typically 4 mm in diameter with a center-to-center interelectrode spacing of 10 mm. To identify subjects with appropriate electrode coverage over the posteromedial cortex (PMC), electrodes were localized on individual high-resolution 3D cortical surfaces. To coregister brain anatomy and electrode location, postoperative head CT images were aligned to preoperative structural T1-weighted MRI whole-brain scans separately for each subject. Anatomical MRI data were reoriented to anterior commissure (AC)-posterior commissure (PC) space by manually identifying the AC, the PC, and a third point in the midsagittal plane. MRI data were then resampled to 1-mm isotropic voxels using a b-spline image interpolation algorithm from SPM5 (http://www.fil.ion.ucl.ac.uk/spm). Postoperative CT images that clearly resolved the location of implanted electrodes were then aligned to the T1 MRI anatomy scans using a mutual information algorithm from SPM5. After CT-MRI alignment, electrodes were identified in the coregistered CT image slices and their centroid coordinates recorded (subject T1 headspace).

To account for minor postoperative shifts in brain position relative to the cranium, electrode coordinates were accordingly adjusted based on a local cortical surface projection, as previously described (1). Cortical surfaces were constructed via manual segmentation of the T1 MRI image using ITKGray, an image segmentation tool based on ITKSnap, and the Stanford University mrVista package (http://white.stanford.edu/software). Electrodes were then visualized on each subject's 3D cortical surface using this segmentation (Fig. S2). Acquiring high-resolution structural imaging in each subject allowed us to construct accurate 3D visualizations of electrode locations relative to each subjects head space within a few millimeters (~5 mm) of error. This process additionally allowed for accurate anatomical identification of electrodes based on clear gyral and sulcal landmarks within each subject to classify PMC coverage, as formally defined in Fig. 1. The accuracy of reconstructed electrode locations was also validated by intraoperative photography as well as electrical brain-mapping logs. For group data each subject's brain was aligned to the same Montreal Neurological Institute template brain (colin27).

Data Recording and Analysis. Electrocorticographic (ECoG) recordings were acquired from implanted strip and grid electrodes by using a multichannel research system (Tucker Davis Technologies) sampled at 3,052 Hz. Data were filtered between 0.5 and 300 Hz and acquired continuously during the experimental task, referenced to the most electrographically silent ECoG channel, and subsequently rereferenced off-line for data analysis. To accurately mark trial timing, a photodiode sensor was placed on the screen of the presentation laptop to trigger each trial event of interest and was time-locked with the ECoG recording. Behavioral responses were logged locally on the presentation laptop. All data processing was performed off-line using custom routines in MATLAB (MathWorks).

Electrode selection. Across the eight subjects, a total of 668 ECoG electrodes were recorded (Table S1). Electrodes showing epileptiform activity or located within the epileptic region were excluded along with electrodes containing excessive noise. Under these conservative criteria, 420 electrodes were included for further data analysis. Electrodes of interest were selected based on formal anatomical and functional criteria. Using the anatomical criteria described in Fig. 1, a total of 33 electrodes (15 left hemisphere; 18 right hemisphere) were judged to be within the boundaries of the PMC and were the focus of our data analysis. Functionally, we first identified responsive electrodes (increase or decrease; described below) within the PMC for all conditions. Subsequently, we found that these changes across conditions were confined to a subset of electrodes that had a consistent profile of response, which were the focus of our initial analysis. Preprocessing and time-frequency methods used for this selection are defined below. Together, these criteria yielded 11 electrodes of interest (reflecting 33% of PMC electrodes; 2.6% of all clean electrodes), which included at least one electrode from each subject (Fig. S4). As detailed below and in the main text, all key findings, specifically all correlative results, were performed across all PMC electrodes so as to control for biasing via electrode selection.

Preprocessing. After anatomical electrode selection, but before response screening, data were notched filtered for 60 Hz line noise and its harmonics. The filtered data were then rereferenced within each subject to a common average of all clean electrodes. All subsequent analyses are based on this preprocessed data.

Time-frequency analysis. Event-related changes in power were initially studied for a wide range of frequencies (1–200 Hz) and then more specifically for band limited changes. Event-related spectral perturbation (ERSP) plots were created for all PMC electrodes across all conditions locked to both stimulus onset and subject response (RT). In addition to the electrode exclusion criteria described above, individual trials were also rejected for amplitude or duration outliers. Any trial with a duration shorter than 800 ms or longer than 12 s was excluded. Additionally, any trial showing transient spike activity, not previously identified, was excluded. These events were excluded if they were greater than 5 SD from the mean of the overall time series. On average these criteria rejected an additional 1.7% of the total number of trials. As previously reported (2), ERSP plots were created using a standard decomposition technique that estimates the normal-

ized power for multiple center frequencies (1–200 Hz) via a Hilbert transform and standardizes these power changes relative to a surrogate null distribution (z-score; see ref. 2 for details). However, for functional electrode selection and the bulk of analysis we focused on the event-related changes in broad high γ-frequency power (HG; 70–180 Hz).

For the screening of responsive electrodes, we used the surrogate normalized time-frequency representation of power to judge if electrodes surpassed a threshold (positively or negatively) for each condition. For each electrode, we averaged the z-score value of power for the 70–180 Hz frequency range to see if it was beyond the 75 percentile (two-sided) of the normalized surrogate distribution ($z > 1.15 \mid < -1.15$). The initial time window of estimation was 500 ms in length and fixed between −700 ms and −200 ms relative to the end of the trial (RT). We focused on time-frequency decompositions averaged relative to RT because trial durations were variable (depended on RT) and, as discussed in the main text, the onset of increased response was no earlier than 400 ms and maximal toward the end of the trial (see Fig. S5 for stimulus-locked responses of Fig. S4). Additionally, a second time window of power estimation was used which was adaptive to the maxima of HG power values because of real variations in power offset latency across electrodes and subjects (as shown in Fig. 4). For the adaptive time-frequency window, the same duration and frequency range was used, but shifted in time to capture the HG power maxima. Additional constraints limited the time-frequency window to within the trial period (could not extend past RT) and not beyond the mean trial duration. The largest mean value from the two time-frequency window estimates was used for analysis (Fig. S3). Subsequently, if an electrode passed the upper threshold (increase) it was designated a 1 and if it passed the lower threshold (decrease) it was designated a −1. Those electrodes that did not pass the threshold were marked 0. These discrete values were then used for accumulating the number of responsive sites for each condition and the overlap between these sites across conditions. Identified electrodes from this process formed the initial functional selection of sites. It is important to note that this selection process served chiefly as a heuristic for data reduction and presentation, and not the central process of statistical inference of task response. Importantly, all key findings reported for the selected self-episodic electrodes are still significant when using all PMC electrodes, as evidenced by statistical comparisons in the text and additional analysis shown below (e.g., Figs. S6 and S7).

After identifying responsive electrodes, we then focused on the specific magnitude and temporal structure of change in the 70–180 Hz range across conditions. Quantitative changes in the broad HG range were estimated by first band-pass filtering the full preprocessed time series between 70 and 180 Hz with a two-way, nonphase-lag, finite impulse response filter from the EEGLAB toolbox (3). A Hilbert transform was then applied to this band-pass signal, with the power then estimated by taking the modulus of the real part (amplitude envelope) from the complex signal and squaring the series. This amplitude time series was then normalized to its overall mean to reflect percentage of signal change from this value. This normalized time series was then smoothed by convolving the data with a 200-ms Gaussian window. All data transforms were performed on the entire experimental time series, with event-related averages estimated by taking epochs from this transformed data, rather than applying filters or transforms to singular short-window segments.

Response latency and duration. Estimation of onset latency for each condition per electrode was calculated using the smoothed HG power (70–180 Hz) described above. Response onset latency was defined by identifying the first supra threshold event (response) during each trial, and then focusing around this time point to accurately identify the latency of its deflection/onset. For each trial a time window extending from 200 ms prior the stimulus onset to the end of the trial was used to identify the first excursion of the HG power above 20% of the mean (threshold). Defining a threshold for the time of activity onset is a trade-off between noise variation (low threshold) and poor latency estimation (high threshold), whereby moving this value higher and higher will ultimately converge to the time-to-peak estimate. We found this 20% threshold to be an optimal trade-off between these factors (note: as described next, the threshold is only used to identify the analysis time window for onset, not the onset time itself). Once identified a smaller window 200 ms before and 100 ms after this supra threshold point was extracted and divided into 20-ms nonoverlapping bins. Each 20-ms bin was then fitted with a least-squares line to estimate the slope of the HG power. Slopes from all of the bins were then ranked ascendingly and the bin with the smallest mean-square error from the top five ranked slopes was selected. The start time of the selected bin defined the response onset latency for each trial (2). An electrode was defined as responsive to a condition if at least 80% of trials were estimated to respond. Median latency and its error were estimated for each electrode and condition. Response offset was estimated with the same approach but moving backward in time from the end of the trial. Finally, it is important to note that this trial-based approach provides a more representative estimation of onset latency, by taking into account real trial-based variations, than similar approaches that simply apply a magnitude threshold to the averaged response.

In addition to estimating the onset and offset of HG response, we also defined the duration of response for both increases and decreases in HG power. Using the same trial-based analysis for latency estimation, the duration of supra threshold responses was logged for each trial and averaged. As trial durations differed, response duration was normalized in time to the percentage of each trial length. Consistent with latency estimates the threshold for increased responses was the duration of HG power >20% of the mean, and for decreased responses the duration of HG power <−20% of the mean.

Statistical Analysis. All statistical analyses of power change were based on normalized values (either z-score relative to a surrogate distribution or percent-change relative to the mean). For comparisons across multiple conditions ANOVA was first used, and when required, followed by post hoc parametric tests of mean difference (t test), with $\alpha = 0.05$ and corrected for multiple comparisons (Bonferroni; α/n tests). Single subject values are expressed as mean ± SD, and for group data mean ± SEM. When normality was violated the data were transformed to a normal distribution.

Experimental Stimuli. All presented task stimuli for each condition are given below.

Self-episodic condition. "I wore white socks yesterday," "I ate pizza this week," "I used a computer today," "I ate breakfast today," "I made my bed this morning," "I was on a highway today," "I drove a car today," "I ate a fruit today," "I read a book this week," "I ate at a restaurant this week," "I had chicken for dinner yesterday," "I watched TV today," "I went shopping this week," "I drank coffee this morning," "I talked on the phone today," "I took a shower this morning," "I went to the movies this week," "I read a newspaper today," "I spent money today," "I listened to music today," "I washed dishes yesterday," "I talked to a relative this morning," "I wore jeans yesterday," "I slept well last night," "I woke up early this morning," "I listened to the radio today," "I went to bed early last night," "I took a nap today," "I cooked dinner last night," "I went dancing this week," "I went to the beach this week," "I read a book this week," "I watched a sports game this week," "I went swimming this week," "I checked my email this morning," "I played with a dog this week," "I bought a CD this week," "I ate a burrito this week," "I

went to the mall this week," "I drank juice this morning," "I went on a walk today," "I rented a movie this week," "I read a magazine yesterday," "I ate candy yesterday," "I went to the bank yesterday," "I played a video game this week," "I worked out this week," "I did my laundry this week."

Self-semantic condition. "I usually wear white socks," "I eat pizza often," "I use computers often," "I usually eat breakfast," "I often make my bed," "I drive on highways often," "I drive a car," "I eat fruit often," "I read books often," "I eat at restaurants a lot," "I eat chicken often," "I watch a lot of TV," "I go shopping often," "I drink coffee often," "I talk on the phone a lot," "I take showers in the morning," "I go to the movies often," "I read the newspaper," "I spend a lot of money," "I listen to music often," "I wash dishes," "I talk to my family often," "I wear jeans often," "I am a deep sleeper," "I usually wake up early," "I listen to the radio," "I usually go to bed early," "I take naps often," "I usually cook dinner," "I dance often," "I go to the beach sometimes," "I read books often," "I watch sports games," "I swim sometimes," "I check my email often," "I have a dog," "I buy a lot of CDs," "I eat burritos often," "I go to the mall a lot," "I drink juice often," "I go on walks often," "I rent a lot of movies," "I read magazines," "I eat a lot of candy," "I go to the bank often," "I play video games often," "I work out a lot," "I do my laundry often."

Self-judgment condition. "I am a quiet person," "I am an emotional person," "I am a loving person," "I am generous," "I am a relaxed person," "I am a good listener," "I am funny," "I am talkative," "I am polite," "I am honest," "I am competitive," "I am a patient person," "I am a quick learner," "I am friendly," "I am a moody person," "I am a happy person," "I am easily upset," "I am easily stressed," "I am a focused person," "I am easily distracted," "I am a demanding person," "I am very thoughtful," "I am very observant," "I am a confident person," "I am a curious person," "I am compassionate," "I am a nurturing person," "I am creative," "I am easily bored," "I am easily scared," "I am shy," "I am dependable," "I am kind," "I am outgoing," "I am helpful," "I am sensitive," "I am hard-working," "I am easily frustrated," "I am a silly person," "I am a caring person," "I am lazy," "I am a selfish person," "I am controlling," "I am a rude person," "I am respectful," "I am smart," "I am a serious person," "I am easily disappointed."

Math condition. "8 + 65 = 73", "51 + 6 = 57", "68 + 7 = 75", "9 + 23 = 34", "47 + 8 = 55", "54 + 4 = 58", "38 + 6 = 42", "5 + 87 = 92", "28 + 6 = 34", "1 + 41 = 42", "61 + 2 = 63", "31 + 8 = 39", "20 + 4 = 24", "45 + 9 = 54", "33 + 5 = 38", "29 + 4 = 33", "81 + 5 = 86", "6 + 39 = 47", "46 + 3 = 49", "78 + 2 = 80","2 + 60 = 72", "7 + 43 = 50", "3 + 89 = 94", "8 + 30 = 38", "4 + 25 = 29", "24 + 5 = 29", "82 + 8 = 90", "26 + 7 = 34", "59 + 7 = 66", "42 + 6 = 48", "9 + 86 = 95", "6 + 36 = 42", "4 + 49 = 53", "5 + 63 = 68", "27 + 3 = 30", "2 + 52 = 56", "48 + 7 = 65", "1 + 18 = 19", "32 + 8 = 40", "3 + 75 = 78", "44 + 9 = 53", "7 + 34 = 42", "16 + 8 = 24" "50 + 9 = 59", "58 + 3 = 61", "6 + 22 = 28", "77 + 4 = 83", "56 + 9 = 65".

SI Discussion

Neural Population Response. It should be noted that the broadband HG range (70–180 Hz) signal that we have recorded intracranially likely reflects the level of population spiking in the local cortical tissue underlying each electrode (4–7). Consistent with this view, the spatial distribution of event-related changes in ECoG HG power are often highly focal and accurately capture functional neuroanatomy, a feature less commonly observed for low-frequency rhythms (< 40 Hz) (8, 9). Moreover, there is an increasing body of evidence suggesting that this HG range is a reliable correlate of changes in blood oxygenation level-dependent activity observed with functional imaging studies (10). In light of these observations, we believe the use of broadband HG ECoG activity as a main dependent measure of local population activity is justified. Given the exposed size of our recording electrodes (~2.3 mm in diameter), the cortical tissue underneath each site will contain ~500,000 neurons (11). Thus, the electrophysiological signals we have measured reflect the activity emanating from local neural populations specific to the anatomical location of electrodes on each subject's cortical surface.

Network Anticorrelation. As a natural extension of the local response properties we have reported, the anticorrelation of activity within the PMC across conditions more broadly reflects the commonly observed anticorrelation of the default mode network (DMN) with the dorsolateral networks of attention (12, 13). Activation of subregions within the lateral parietal cortex is commonly observed for attentionally demanding conditions associated with DMN suppression (12, 14). As noted in the discussion, it is therefore of great interest to further probe this task driven anticorrelation electrophysiologically, particularly between the medial and lateral aspects of the parietal lobe. Such efforts will require additional focus toward subdivisions within networks, given recent evidence against a simple uniformity of response across DMN midline structures (15–17).

Anatomical Coverage. Importantly, we note that our coverage of the PMC, although reflecting a great increase from previous reports in the literature, does contain relatively few recording sites in the precuneus/7m region. Therefore, our conclusions regarding PMC activity require the addition of precuneus recordings to allow for a more comprehensive mapping of this regions functional neuroanatomy. One final anatomical note is the lack of laterality observed. Although neuroimaging data suggests a left hemisphere dominance of episodic memory effects and of the DMN more generally, we did not find any hemispheric differences. However, this null result should be interpreted cautiously, because the sampling of each hemisphere, although similar in number (Electrode# L:15, R:18), was not anatomically matched.

1. Hermes D, Miller KJ, Noordmans HJ, Vansteensel MJ, Ramsey NF (2010) Automated electrocorticographic electrode localization on individually rendered brain surfaces. *J Neurosci Methods* 185:293–298.
2. Dastjerdi M, et al. (2011) Differential electrophysiological response during rest, self-referential, and non-self-referential tasks in human posteromedial cortex. *Proc Natl Acad Sci USA* 108:3023–3028.
3. Delorme A, Makeig S (2004) EEGLAB: An open source toolbox for analysis of single-trial EEG dynamics including independent component analysis. *J Neurosci Methods* 134:9–21.
4. Miller KJ (2010) Broadband spectral change: Evidence for a macroscale correlate of population firing rate? *J Neurosci* 30:6477–6479.
5. Manning JR, Jacobs J, Fried I, Kahana MJ (2009) Broadband shifts in local field potential power spectra are correlated with single-neuron spiking in humans. *J Neurosci* 29:13613–13620.
6. Ray S, Crone NE, Niebur E, Franaszczuk PJ, Hsiao SS (2008) Neural correlates of high-gamma oscillations (60–200 Hz) in macaque local field potentials and their potential implications in electrocorticography. *J Neurosci* 28:11526–11536.
7. Ray S, Maunsell JH (2011) Different origins of gamma rhythm and high-gamma activity in macaque visual cortex. *PLoS Biol* 9:e1000610.
8. Miller KJ, et al. (2007) Spectral changes in cortical surface potentials during motor movement. *J Neurosci* 27:2424–2432.
9. Flinker A, Chang EF, Barbaro NM, Berger MS, Knight RT (2011) Sub-centimeter language organization in the human temporal lobe. *Brain Lang* 117:103–109.
10. Hermes D, et al. (2012) Neurophysiologic correlates of fMRI in human motor cortex. *Hum Brain Mapp* 33:1689–1699.
11. Pakkenberg B, Gundersen HJ (1997) Neocortical neuron number in humans: Effect of sex and age. *J Comp Neurol* 384:312–320.
12. Fox MD, et al. (2005) The human brain is intrinsically organized into dynamic, anticorrelated functional networks. *Proc Natl Acad Sci USA* 102:9673–9678.
13. Fransson P (2005) Spontaneous low-frequency BOLD signal fluctuations: An fMRI investigation of the resting-state default mode of brain function hypothesis. *Hum Brain Mapp* 26:15–29.

14. Corbetta M, Shulman GL (2002) Control of goal-directed and stimulus-driven attention in the brain. *Nat Rev Neurosci* 3:201–215.
15. Spreng RN, Stevens WD, Chamberlain JP, Gilmore AW, Schacter DL (2010) Default network activity, coupled with the frontoparietal control network, supports goal-directed cognition. *Neuroimage* 53:303–317.
16. Andrews-Hanna JR, Reidler JS, Sepulcre J, Poulin R, Buckner RL (2010) Functional-anatomic fractionation of the brain's default network. *Neuron* 65:550–562.
17. Leech R, Kamourieh S, Beckmann CF, Sharp DJ (2011) Fractionating the default mode network: Distinct contributions of the ventral and dorsal posterior cingulate cortex to cognitive control. *J Neurosci* 31:3217–3224.

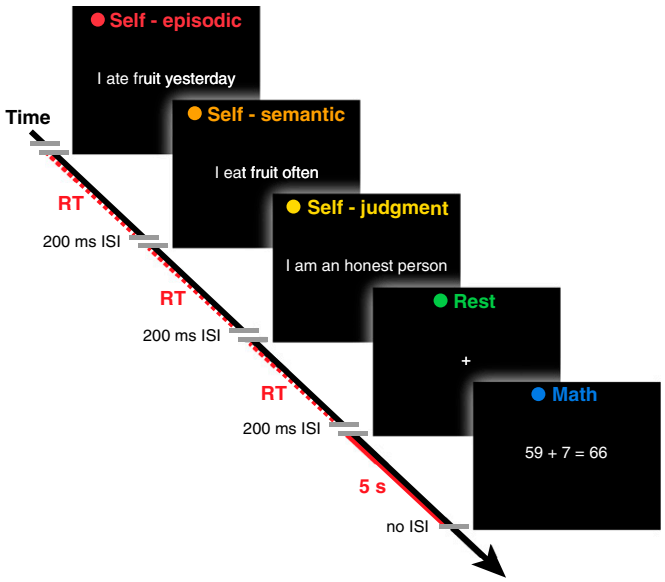

Fig. S1. Experimental task. Subjects were asked to judge the accuracy (true/false) of sentences and equations and report their response by pressing either "1" or "2" on a keypad corresponding to true or false, respectively. For these response conditions trials were self-paced with varying RT duration. These stimuli were interleaved with a randomly occurring rest condition that lasted for a fixed 5 s. The interstimulus interval (ISI) consisted of a blank screen shown for 200 ms, except for after rest trials, where there was no ISI. All stimuli were presented in white font centered on a black background.

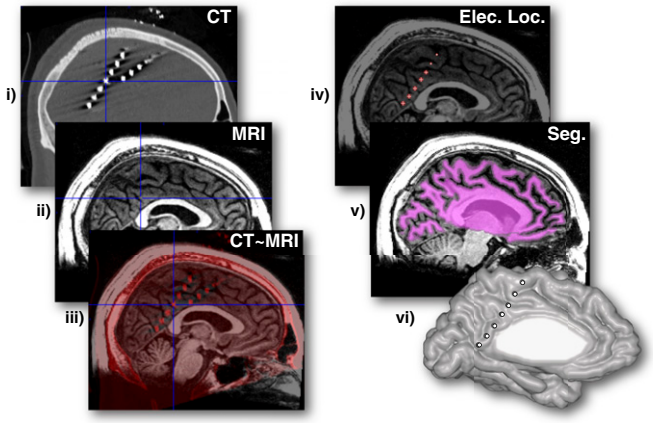

Fig. S2. Localization of electrodes using CT-MRI fusion. The location of recording electrodes on the cortical surface was determined by registering the postimplant CT image with a high-resolution preoperative T1 anatomical MRI scan (*i–iii*). After this alignment, electrode coordinates for each strip or grid electrode array were localized separately within the individual subjects MRI head space (*iv*). These coordinates were then located upon the cortical surface extracted from a manual segmentation of the MRI white matter with a cortical layer expansion (*v* and *vi*).

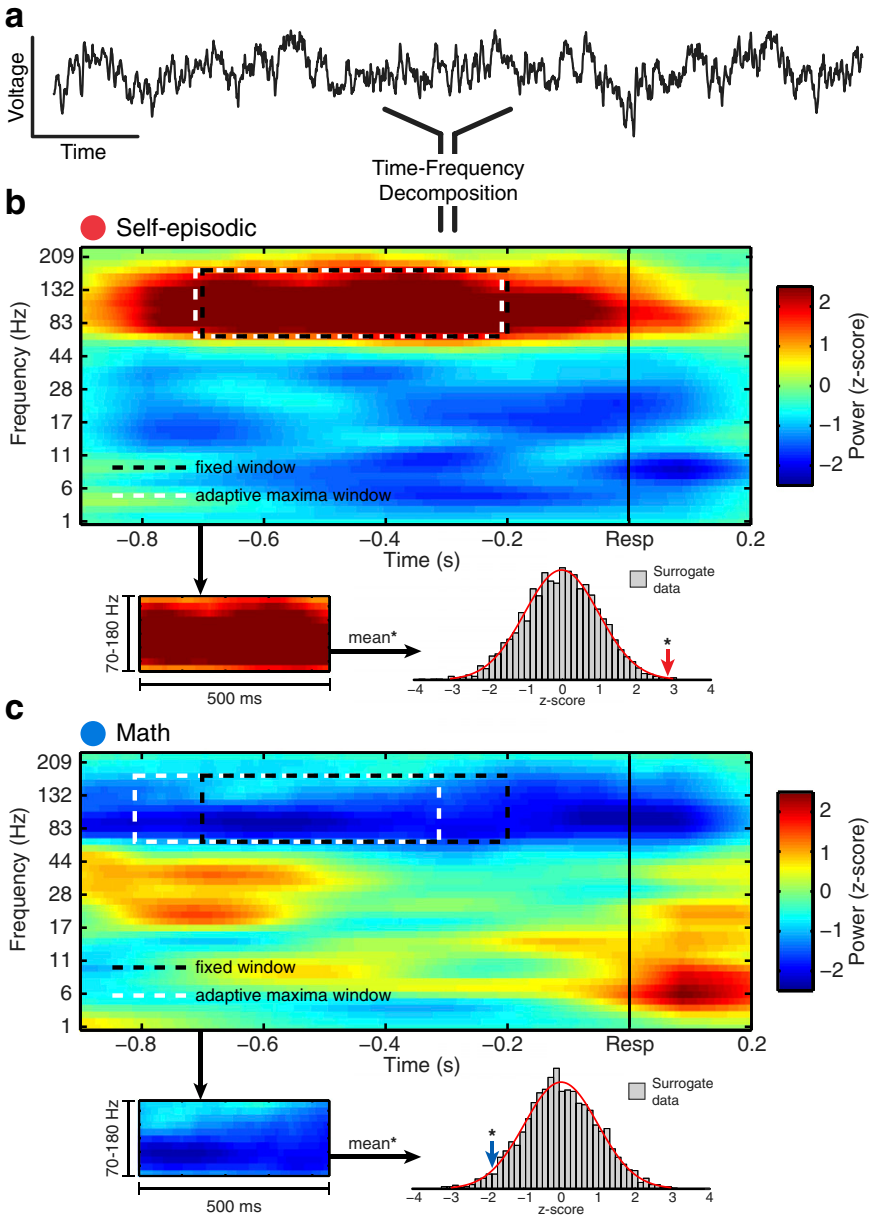

Fig. S3. Time-frequency analysis and response estimation. (*A*) Preprocessed time series for each electrode were decomposed into a time-frequency power (spectrogram) representation (example data from subject 1). Event-related time-frequency changes in power (ERSPs) were estimated by normalizing the mean event-related time-frequency matrix to a matching surrogate distribution at each time-frequency position. To define increased (*A*, self-episodic example) or decreased (*B*, math example, same electrode) responses the mean HG power (70–180 Hz) for a fixed-length 500-ms window was calculated. Because the timing of ERSPs necessarily differed between subjects, we estimated the power for a fixed-latency window (black-dashed box) and also for an adaptive window (white-dashed box), which was shifted to the absolute maxima of power change (both 500 ms in length and limited within the trial period; see *SI Materials and Methods*). The highest mean value between these two estimates was used. As this mean reflects a normalized value relative to some null distribution, responsive electrodes (increase or decrease) were judged by those mean values falling beyond (two-tailed) the 75% percentile (z-score ± 1.15) of the surrogate distribution. Importantly, this process was for responsive electrode selection and not as a final test of significance of response.

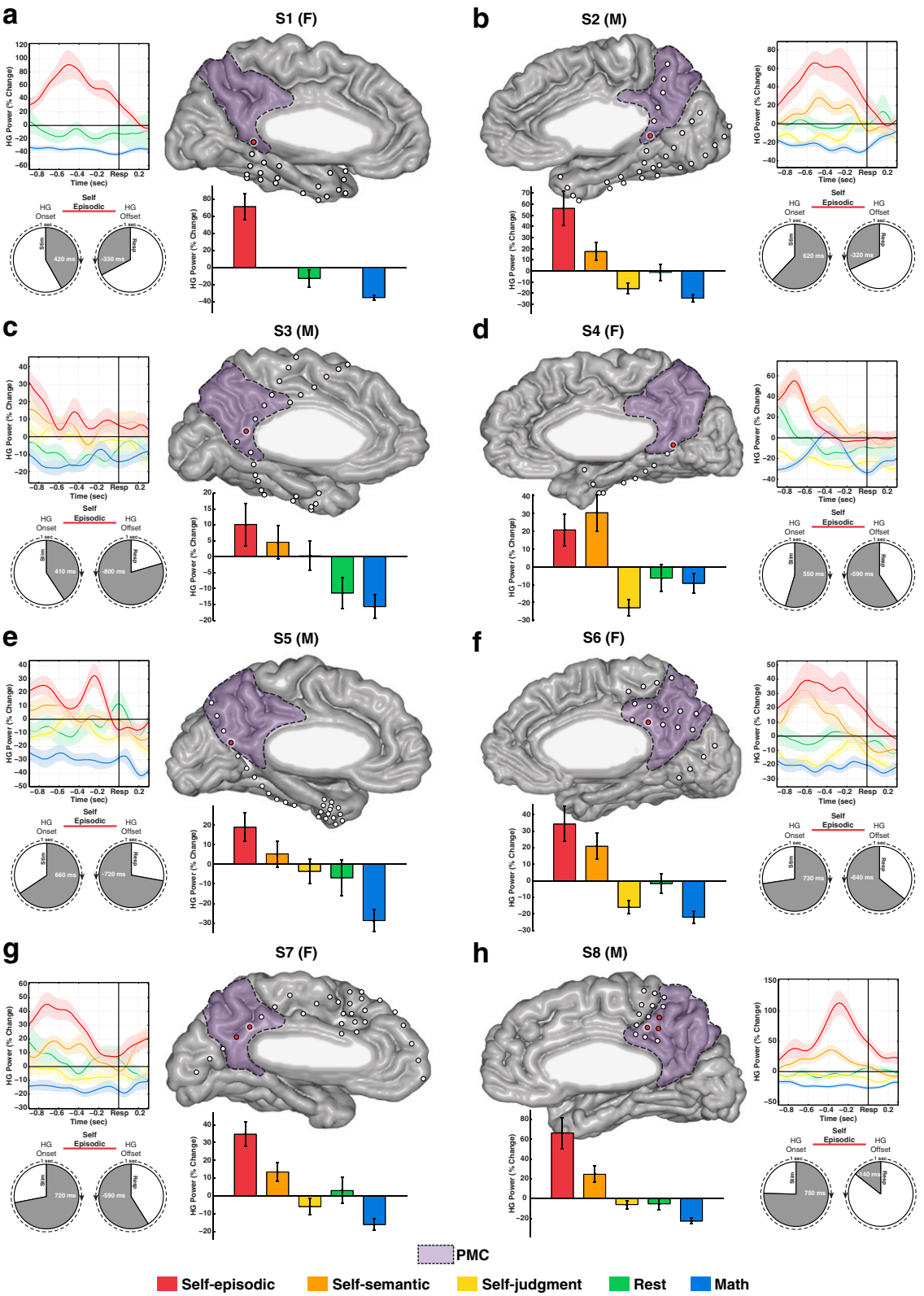

Fig. S4. Event-related changes in HG power across conditions and subjects. For each subject (S) [either female (F) or male (M)] there is a subplot containing four panels. Left-hemisphere subjects are shown on the left (*A*, *C*, *E*, *G*) and right-hemisphere subjects are shown on the right (*B*, *D*, *F*, *H*). Each subject panel displays the rendered cortical surface and the location of electrodes in that particular subject's own brain space. The PMC (purple fill) is demarcated by anatomical boundaries defined in Fig. 1. Electrodes identified as significantly responsive are shown with red fill, with an example responsive electrode selected for each subject with white halo (used for all other panels). For each subject, we have shown the response-locked average of HG power for all conditions (see condition legend at the bottom of the figure; note: subject 1 did not complete all conditions). The shaded area around each trace represents the SD of the HG power. For each subject, five bars with five different colors show the response-locked HG power (with SD) for five different conditions (selected electrode). The pie

Legend continued on following page

charts for each subject are the "latency clocks" for only the self-episodic condition. These clocks show either the onset latency of HG power (locked to stimulus; *Left* clock) or the offset latency of HG power (locked to response; *Right* clock). For example, in subject 1 HG activity begins to increase 420 ms after the onset of self-episodic sentences (e.g., "I used a computer today"). This activity begins to subside ~330 ms before the subject responds with a key press if the sentence is true or false. Note that electrodes in the more ventral PMC have shorter response onset latencies. This is shown in more detail in Fig. 4.

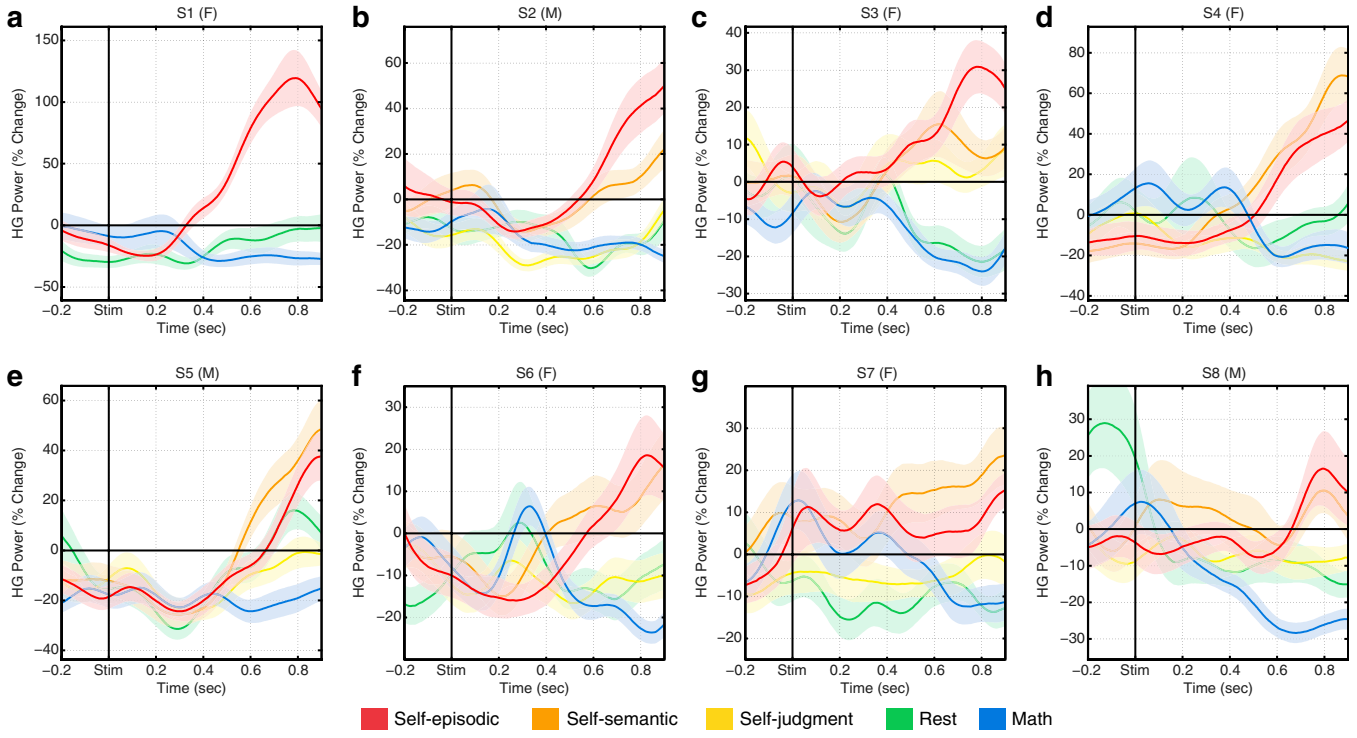

Fig. S5. Event-related changes in HG power across conditions locked to onset. Because of variable trial duration and late onset of HG response (see Fig. 4), RT-locked data were used for most analyses. However, as shown above the divergence of response across conditions can still be seen in stimulus-locked broad HG power. (*A–H*) Stimulus-locked HG traces for each subject matched to electrodes responses shown in Fig. S2. Plots show change in the HG power (percent change from mean) on the *y* axis across time (*x* axis) and locked to stimulus presentation (Stim.). Interestingly, there is a consistent latency of divergence for self-episodic and math conditions.

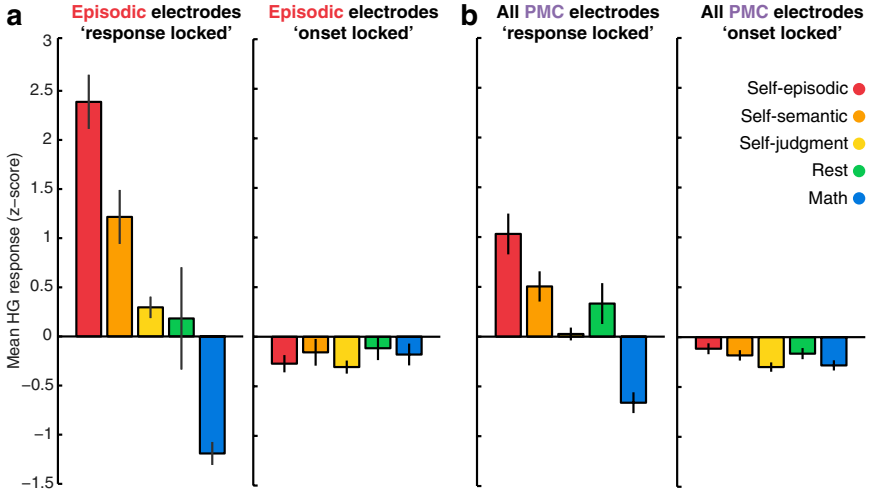

Fig. S6. Mean HG response magnitude for self-episodic electrodes and all PMC electrodes, across all conditions, for both response-locked and onset-locked data. Mean HG response across all conditions is shown for electrodes that were identified as responsive during the self-episodic condition (*A*), and for all PMC electrodes (*B*). For both *A* and *B*, *Left* plots show mean HG magnitude observed for the late response locked window; *Right* plots show mean HG magnitude observed for the early onset locked window. Data clearly show that the changes across conditions observed for the self-episodic response electrodes were also observed when grouping all PMC electrodes (although means are attenuated because of the inclusions of non/weak response electrodes). Furthermore, these event-related changes across conditions were only observed for the late response locked analysis (see *SI Materials and Methods*).

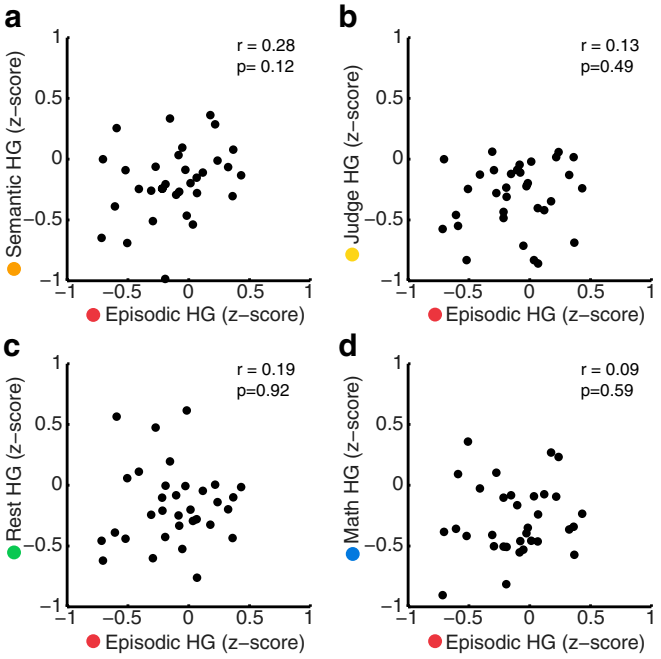

Fig. S7. Onset-locked response magnitude shows no correlation across conditions. Scatter correlation plots of mean HG response for all PMC electrodes (same as Fig. 2) for onset-locked magnitudes. Using the same approach as response-locked analyses, we obtained HG responses for stimulus onset data (0–300 ms). As predicted, data from this time window did not show any significant correlations across conditions when comparing the self-episodic condition with self-semantic (*A*), self-judgment (*B*), rest (*C*), and math (*D*) conditions, respectively.

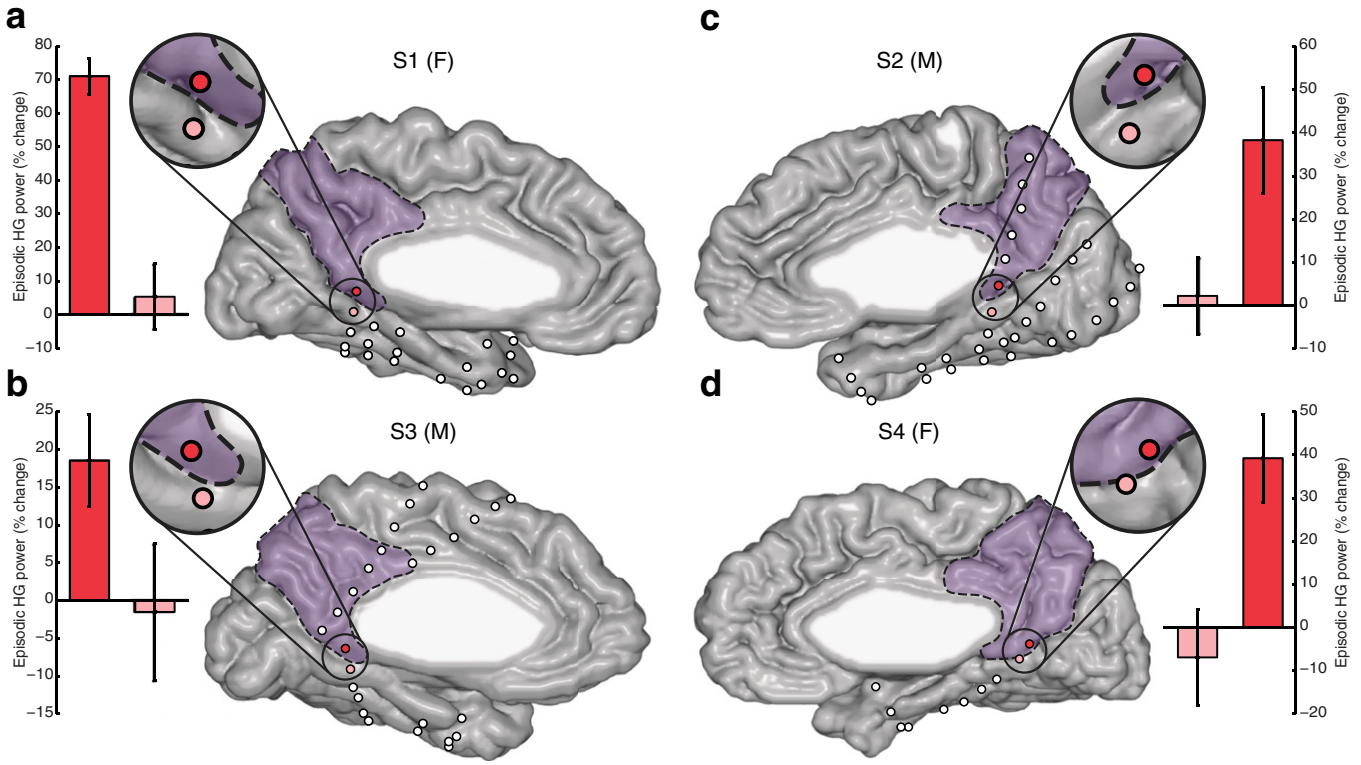

Fig. S8. Functional response within the PMC bounded by its anatomical borders. (*A–D*) Four of eight subjects had interhemispheric electrode strips that clearly crossed the border between the PMC (purple fill) and the parahippocampal gyrus (*A* and *B* are left hemisphere; *C* and *D* are right hemisphere). At the site of boundary crossing, the response to the self-episodic memory condition is shown for two electrodes located on either side of this boundary (dark red within PMC; light red outside PMC). Responses are shown as HG percentage change (from mean) with SD. The edge-to-edge distance of these electrode pairs was ~6 mm.

Table S1. Single subject clinical data

Subject	Sex	Age (y)	Hemisphere	Electrode no. (total)	Electrode no. (clean)	Seizure focus	Resection (Y/N)	FSIQ	VIQ	PIQ
1	F	21	Left	68	8	L: med/lat. temporal lobe	Y	89	89	91
2	M	46	Right	112	103	R: calcarine sulcus	N	106	106	104
3	M	39	Left	114	97	L: Insula	Y	94	102	87
4	F	22	Right	54	34	R: med. temporal lobe	Y	100	94	106
5	M	31	Left	118	43	L: med/lat. temporal lobe	Y	80	62	104
6	F	32	Right	64	34	R: med. occipital lobe	Y	95	95	96
7	F	43	Left	64	39	L: med. temporal lobe	Y	73	67	85
8	M	34	Right	74	62	R: med. precentral gyrus	N	124	119	121
Mean		34	Total	668	420	—	Mean	95.16	91.75	99.25
SD		9.1	—	—	—	—	SD	15.73	19.17	11.93

Tabulation shows basic subject statistics for sex, age, hemisphere of implantation, total electrodes implanted, total clean electrodes (for analysis), seizure focus, subsequent surgical resection, and neuropsychological evaluation results. Abbreviations: FSIQ, full scale intelligence quotient; PIQ, performance intelligence quotient; VIQ, verbal intelligence quotient.